Status and Outlook of Operational Satellite Precipitation Algorithms for Extreme-Precipitation Events

RODERICK A. SCOFIELD AND ROBERT J. KULIGOWSKI

National Environmental Satellite, Data, and Information Service, Camp Springs, Maryland

(Manuscript received 17 October 2002, in final form 13 May 2003)

ABSTRACT

Flash floods are among the most devastating natural weather hazards in the United States, causing an average of more than 225 deaths and $4 billion in property damage annually. As a result, prediction of flash floods in an accurate and timely fashion is one of the most important challenges in weather prediction. Data from geostationary and polar-orbiting satellites are significant sources of information for the diagnosis and prediction of heavy precipitation and flash floods. Geostationary satellites are especially important for their unique ability simultaneously to observe the atmosphere and its cloud cover from the global scale down to the storm scale at high resolution in both time (every 15 min) and space (1–4 km). This capability makes geostationary satellite data ideally suited for estimating and predicting heavy precipitation, especially during flash-flood events. Presented in this paper are current and future efforts in the National Environmental Satellite, Data, and Information Service that support National Weather Service River Forecast Centers and Weather Forecast Offices during extreme-precipitation events.

1. Introduction

Flash-flood forecasting represents one of the most serious challenges to the operational forecasting and research communities because of the high toll of flash flooding in terms of human life (more than 225 fatalities on average each year in the United States alone) and property damage ($4 billion per year in the United States). Timely and reliable information on recent, current, and future precipitation is thus vital for enabling forecasters to make accurate and timely forecasts and to warn the public appropriately.

Rain gauges have been a primary source of precipitation data for well over a century. Although rain gauge data have the clear advantage of representing a direct measurement of precipitation (as opposed to an estimate obtained by relating precipitation to some remotely sensed quantity), rain gauges also exhibit a number of significant shortcomings for flash-flood forecasting purposes. The poor spatial resolution of the rain gauge network is the most obvious shortcoming: Smith et al. (1994, 1996) have demonstrated by comparisons with radar that even relatively dense existing rain gauge networks are unable to depict the intensity and spatial extent of heavy precipitation. Undercatch caused by wind effects (as well as by mechanical limitations in the case of tipping-bucket gauges) can also be significant during heavy-precipitation events (e.g., Groisman and Legates 1994; Peck 1997).

The advent of radar as a tool for estimating precipitation addressed these issues to some extent by providing widespread spatial coverage at high spatial and temporal resolution (though proximity to a radar unit was still necessary) and by providing spatially continuous values instead of point measurements. However, transformation of the radar-measured reflectivities into rainfall rates presents difficulty in three areas. The first area is the accuracy of the reflectivity values themselves, which can be affected by influence from fixed targets (e.g., ground clutter, beam block) or by the intermittent influence of anomalous propagation (which is exceedingly difficult to diagnose and remove when precipitation is occurring). Differences in calibration among radars are also a serious problem: Hunter (1996) noted that a difference of 1 dBZ in calibration translates to a 17% difference in rain rate, and Smith et al. (1996) found a difference of 44% in mean cold-season rainfall between the Tulsa and Twin Lakes, Oklahoma, radars.

Second, the increase in elevation of the beam with distance from the radar leads to errors associated with uncertainties in the shape of the reflectivity profile between the beam height and the surface; precipitation is often undetected, or the rate is underestimated, as distance from the radar increases (Hunter 1996; Kitchen and Jackson 1993; Smith et al. 1996). These difficulties are especially pronounced in mountainous regions, where the placement of the radar at a high elevation to

Corresponding author address: Dr. Roderick A. Scofield, E/RA2, RM 601, WWBG, 5200 Auth Rd., Camp Springs, MD 20746-4304. E-mail: roderick.scofield@noaa.gov

minimize beam block results in significant nondetection of precipitation, especially at longer ranges (Westrick et al. 1999; Young et al. 1999). On the other hand, brightband effects where the radar beam intercepts the melting layer can lead to overestimation of rainfall rates at short to intermediate ranges (Kitchen and Jackson 1993; Smith at al. 1996). In addition to these uncertainties about the reflectivity value and its relationship to surface conditions, the relationship between reflectivity and rainfall rate—commonly referred to as the Z–R relationship—is related to the drop size distribution and is also affected by beam spreading because a uniform spatial distribution of liquid drops is assumed (Hunter 1996).

Numerous efforts have been made to address these issues. Range corrections based on knowledge of the beam spread with distance have been implemented but, as Fulton et al. (1998) note, the beam-spread contribution to range effects is minor in comparison with the contributions from beam overshooting and nonuniformity of the vertical reflectivity profile. Vertical profile adjustments have been proposed (e.g., Seo et al. 2000 and references therein), but they assume horizontal homogeneity in the vertical variations of reflectivity, and, more important, precipitation must be detected by the radar for such corrections to be performed. Gauges have been used to correct biases in the radar fields in real time, such as in the Stage-III and P1 products produced by River Forecast Centers (RFC; Fulton et al. 1998) and in experimental procedures (e.g., Gourley et al. 2002; Seo and Breidenbach 2002); however, these bias corrections are unable to address range and other effects completely (Young et al. 2000).

Satellite precipitation estimates (SPEs) offer an excellent way to compensate for some of the limitations of other sources of quantitative precipitation information. SPEs cover the entire contiguous United States and surrounding regions at 4-km resolution every 15 min, are uninhibited by mountains and other obstacles, and do not exhibit the spatial inconsistencies that affect radar, such as calibration differences and changes in radar beam height. However, it is also clear that the relationship between satellite-measured radiances and rainfall rates is less robust than that between radar reflectivities and rainfall rates; as a consequence, SPEs must not be considered as a replacement for radar estimates and gauges but as a complement.

A follow-up to a recent article (Scofield 2001) is now presented that describes the status and outlook of operational satellite precipitation algorithms for extreme precipitation events. From 1978 through 2000, SPEs for flash floods were produced using data from the Geostationary Operational Environmental Satellite (GOES) solely by a combination of manual effort and computer algorithms through the Interactive Flash-Flood Analyzer (IFFA), and their primary application was to alert forecasters and hydrologists of the potential for heavy precipitation and flash floods. For the past several years, efforts have been focused on automating SPEs to increase both their timeliness and their applicability. In addition to their current status as an alert tool, SPEs will one day be directly incorporated into a number of prediction estimation and forecasting products, including

- the multisensor precipitation estimate, which will replace Stage III (Fulton et al. 1998);
- hydrologic models that are run at local RFCs;
- numerical weather prediction models—to improve quantitative precipitation forecasts (QPFs);
- cloud models that in turn will provide precipitation estimates; and
- 1–3-h nowcasting algorithms.

Section 2 of this paper contains an overview of satellite algorithms, and section 3 briefly describes three GOES-based quantitative precipitation estimation (QPE) algorithms currently run at the National Environmental Satellite, Data, and Information Service (NESDIS) in real time: the IFFA, Autoestimator/Hydroestimator (AE/HE), and GOES multispectral rainfall algorithm (GMSRA), respectively. The performance of satellite QPE is illustrated in section 4 using two case studies, followed by discussion of future research directions in section 5.

2. A brief history of satellite QPE algorithms

Although the scope of this paper is restricted to applications of satellite QPE for extreme events, the pioneering work in satellite QPE involved large scales in time and space and hence will be mentioned briefly. The reader is referred to more comprehensive reviews of satellite precipitation algorithms in Barrett and Martin (1981), Scofield (1991), Petty (1995), Petty and Krajewski (1996), and World Meteorological Organization (1999).

a. Infrared-/visible-based estimates

Techniques for estimating precipitation from infrared and/or visible satellite data have existed almost as long as the data have been available. Rainfall rates are generally derived from cloud-top infrared (IR) brightness temperature, which is related to cloud-top height for optically thick clouds below the tropopause. This relationship assumes that the cloud height is related to cloud thickness—an assumption that holds reasonably well for active convective clouds but is problematic for nimbostratus clouds (for which rain rates are often underestimated because of the relatively warm cloud tops) and nonprecipitating cirrus clouds (which may be incorrectly identified as precipitating clouds because of their low brightness temperatures).

Early research using data from polar-orbiting satellites (prior to the era of geostationary satellites) pursued a wide range of avenues, including relating 3-h precip-

itation probability to IR window brightness temperature (Lethbridge 1967), estimating daily rainfall from visible (Follansbee 1973) and IR (Follansbee and Oliver 1975) data, and estimating monthly rainfall based on nephanalyses (charts of cloud type and coverage) constructed from polar-orbiting satellite overpasses (Barrett 1970).

The advent of geostationary satellites made IR/visible-based SPEs useful for operational evaluation of extreme-precipitation events, because the time interval involved (15 min at present) is much more compatible with the time scale of these events than the time interval between the overpasses of a polar-orbiting satellite. This dramatic increase in the availability of IR and visible imagery was accompanied by a similarly dramatic increase in the number of techniques for retrieving precipitation estimates from these data. The more notable algorithms include the so-called Griffith–Woodley technique (Griffith et al. 1978); the GOES precipitation index (Arkin and Meisner 1987), and the convective–stratiform technique (Adler and Negri 1988). Many of these algorithms were initially developed for large time and space scales, but the scales have become finer as instrumentation has improved and the data-processing capacity has increased.

In this vein, Scofield and Oliver (1977) pioneered the first operationally applied mesostorm-scale algorithms that could be modified for a variety of extreme weather situations (Borneman 1988). Interaction between forecasters and computer algorithms was crucial for the flexibility required by these algorithms, hence the name Interactive Flash-Flood Analyzer. Building on certain aspects of the IFFA system, a fully automated algorithm called the Autoestimator was developed by Vicente et al. (1998, 2002) and is detailed in section 3b along with its follow-up, the Hydroestimator (Kuligowski et al. 2003, manuscript submitted to *Wea. Forecasting*), following a description of the IFFA in section 3a. GMSRA (Ba and Gruber 2001) is another automated algorithm that uses data from all five GOES channels to improve rain/no-rain discrimination and is described in section 3c.

A fairly recent development has been the development of SPE algorithms that use artificial-neural-network techniques, which provide a flexible framework for using information about cloud spatial characteristics instead of simply relying on brightness temperature values alone. Examples of these neural-network methods include Sorooshian et al. (2000) and Zhang and Scofield (1994).

b. Microwave-based estimates

Although the high spatial and temporal resolution of IR/visible data from geostationary satellites make them ideally suited for SPE, the relationship between rainfall rate and the characteristics of the cloud tops is indirect and is best suited for convective precipitation, for which the cloud-top height and cloud depth are somewhat related. These difficulties have led to a body of research into using microwave data to produce SPEs. Because only heavily precipitating clouds are optically thick in the microwave spectrum, information about cloud thickness and water/ice content can be inferred from microwave radiances. This is done using one of two approaches. Emission algorithms compare the emissions of cloud water at low microwave frequencies with the values that would be expected if no cloud were present, which is best done over a radiometrically cold surface such as the open ocean, so that clouds appear to be warm. Scattering algorithms estimate the backscattering of upwelling microwave radiation by ice particles in the clouds by comparing the (low) cloud brightness temperature with the relatively high values that would be observed if no cloud were present.

Early work using the emission approach included that of Savage and Weinman (1975) and Weinman and Guetter (1977), who used 37-GHz data from the Electrically Scanning Microwave Radiometer on the *Nimbus-6* satellite. Spencer (1986) developed a more quantitative algorithm for 37-GHz data from the Scanning Multichannel Microwave Radiometer on *Nimbus-7*. The advent of the Special Sensor Microwave Imager (SSM/I) and, in particular, its introduction of an 85.5-GHz channel led to the development of scattering algorithms that were much more robust over land than were emission algorithms and resulted in substantial improvements in the ability to estimate rainfall from microwave radiance data (e.g., Barrett et al. 1988; Spencer et al. 1989). Since then, numerous algorithms have been developed, and they are summarized in intercomparison papers such as Conner and Petty (1998) and Smith et al. (1998).

At NESDIS, precipitation estimates are routinely produced using data from the SSM/I (Ferraro 1997) and the Advanced Microwave Sounding Unit (AMSU; Ferraro et al. 2000; Weng et al. 2002). Also noteworthy are rain-rate estimates produced routinely from the Tropical Rainfall Measuring Mission (TRMM) Microwave Imager (TMI; Kummerow et al. 1998, 2001).

Despite the time limitations of observations from polar-orbiting satellites, Ferraro et al. (1998, 1999, 2000) have demonstrated that microwave-based SPEs are useful for mesostorm-scale analysis and forecasting. However, the most useful application appears to be in using microwave SPEs in conjunction with GOES data, as detailed in section 2c. TRMM also offers an opportunity to investigate the use of multiple instruments in conjunction for SPE, because the TRMM satellite carries not only the TMI but also a precipitation radar, visible and IR sensors, and a lightning detector.

Microwave SPEs have also proven to be useful as a basis for short-term forecasts of precipitation from landfalling tropical systems. The original technique, developed for GOES data by Spayd and Scofield (1984a), has evolved into an automated tropical rainfall potential (TRaP) technique that combines SSM/I-, AMSU-, and TMI-based estimates of rainfall with storm-track fore-

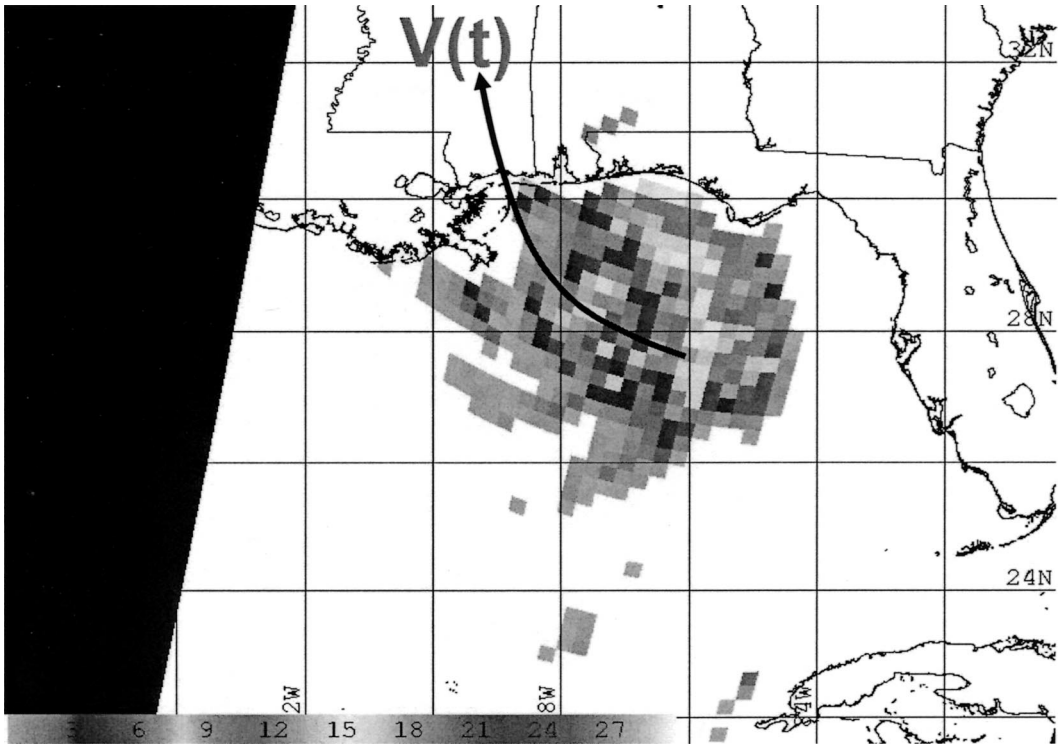

FIG. 1. Schematic of the TRaP algorithm. The predicted rainfall accumulation at a point is computed by integrating the rainfall rate over time along the storm velocity vector **V**(*t*), which is depicted here as a streamline for ease of interpretation.

casts to produce forecasts of 24-h precipitation prior to landfall (World Meteorological Organization 1999; Kidder et al. 2000; Scofield et al. 2001; Ferraro et al. 2002). This process is illustrated in Fig. 1 (examples and experimental real-time products could be found online at the time of writing at http://www.ssd.noaa.gov/PS/TROP/trap-img.html). Operational weather forecasters along the West Coast of the United States have also used microwave-based estimates of precipitation to evaluate the precipitation potential of wintertime storms before they reach land.

c. Estimates blending infrared and microwave data

As stated previously, precipitation estimates from instruments based on GOES and Polar Operational Environmental Satellite (POES) possess a number of complementary strengths and weaknesses. Whereas IR/visible-based estimates from GOES rely only on information from near the top of the cloud (i.e., cloud-top height, and in some cases microphysical information near the cloud top), microwave-based estimates from POES are based on the concentration of water and ice throughout the cloud. However, these estimates are much less frequent and have lower spatial resolution than the GOES data, making the GOES data necessary for analyzing heavy precipitation that occurs at relatively small scales in space and time.

As reviewed in Kuligowski (2002), a number of researchers have recognized the value of combining the relative accuracy of microwave-based estimates of rainfall from polar-orbiting platforms with the nearly continuous availability of infrared-based estimates from geostationary platforms. This melding is typically done by using the more accurate microwave estimates to calibrate and adjust the more indirect GOES-based estimates. Many of the resulting algorithms have been applied only to longer time scales (i.e., 1 month); however, algorithms suitable for short-term application (and thus application to extreme events) have also been developed. These algorithms include those that fit the 10.7-μm brightness temperature to microwave-based rain rates using linear regression (Vicente 1994; Miller et al. 2001), cumulative distribution functions (Manobianco et al. 1994; Turk et al. 1998; Anagnostou et al. 1999; Todd et al. 2001; Huffman et al. 2001), or artificial neural networks (Sorooshian et al. 2000). The self-calibrating multivariate precipitation retrieval (SCaMPR) algorithm developed by Kuligowski (2002) uses a combination of linear regression and discriminant analysis and is capable of using data from multiple GOES channels.

In addition, NESDIS is currently testing and evaluating a form of the Turk et al. (1998) algorithm that has incorporated some of the AE enhancements such the precipitable water/relative humidity adjustment, the ra-

dar-based screening of nonraining cloud pixels, and the parallax adjustment (please refer to section 3b for details on these adjustments). This algorithm uses microwave estimates from SSM/I, AMSU, and TMI for calibration.

3. Real-time GOES-based satellite QPE algorithms at NESDIS

a. Interactive Flash-Flood Analyzer

The National Oceanic and Atmospheric Administration (NOAA)/NESDIS Satellite Analysis Branch (SAB) produces QPE (Borneman 1988; Kuligowski 1997) and outlooks for field forecasters using the IFFA technique (Scofield and Oliver 1977; Scofield 1987). The IFFA, which was designed for intense-precipitation events, uses GOES-based satellite data because of their high spatial and temporal resolution. Though not discussed in this paper, the IFFA techniques have also been developed for winter storms and lake-effect snows (Scofield and Spayd 1984). SAB forecasters determine which portions of convective clouds are active based on changes between successive GOES IR and visible images and then apply the IFFA technique as a basis for drawing isohyets of estimated rainfall from the active clouds. The resulting estimates are adjusted for overshooting cloud tops, cloud mergers, available moisture, low-level inflow, and the speed of the storm. A rain-burst factor helps to account for extremely heavy rainfall that can occur in the incipient stages of a mesoscale convective system (MCS). Also, because the original IFFA algorithm was designed for cold-top convection (colder than -58°C), the convective equilibrium-level temperature is used to adjust for warm tops. For additional details, the reader is referred to Scofield and Oliver (1977) and Scofield (1987).

These QPEs are also extrapolated to produce 3-h precipitation forecasts called nowcasts and outlooks (Spayd and Scofield 1984b), taking into account the growth, decay, movement, and propagation of individual convective systems (Shi and Scofield 1987; Juying and Scofield 1989; Corfidi et al. 1996). SAB SPEs and outlooks are sent out with the advanced weather interactive processing system (AWIPS); at the time of writing, graphics of the estimates are also available online on the Satellite Services Division home page (http://www.ssd.noaa.gov/PS/PCPN/index.html). However, because of the manual and interactive nature of the IFFA method, these SPEs cover limited areas over limited periods of time and can take a significant amount of time to produce.

b. Autoestimator and Hydroestimator

To improve the spatial and temporal coverage of SPEs and increase their timeliness, NESDIS developed an automated SPE algorithm for high-intensity rainfall called the Autoestimator. The original AE, developed by Vicente et al. (1998), computes rain rates from 10.7-μm brightness temperatures based on a curve (Fig. 2) that was derived from more than 6000 collocated radar and satellite pixels. Areas of nonraining cold cloud are identified based on the spatial gradients and time changes of the 10.7-μm brightness temperature field, and amounts are adjusted using a multiplicative moisture adjustment [consisting of precipitable water (PW) in inches multiplied by relative humidity (RH) as a decimal value] based on data from the Eta Model. During 1998 and 1999, a number of enhancements were added to this algorithm: 1) use of 15-min imagery instead of 30-min imagery (note that the IFFA still uses 30-min imagery because production of the estimates is labor intensive), 2) use of 15-min Weather Surveillance Radar-1988 Doppler (WSR-88D) reflectivity data to screen out nonraining cold cloud, 3) an equilibrium-level temperature adjustment (from the Eta Model) for warm-top convection modeled on Scofield (1987) that adjusts brightness temperatures downward (and thus rain rates upward) in regions in which the convective equilibrium level is relatively low (and thus relatively warm), and 4) parallax and orography adjustments (Vicente et al. 2002).

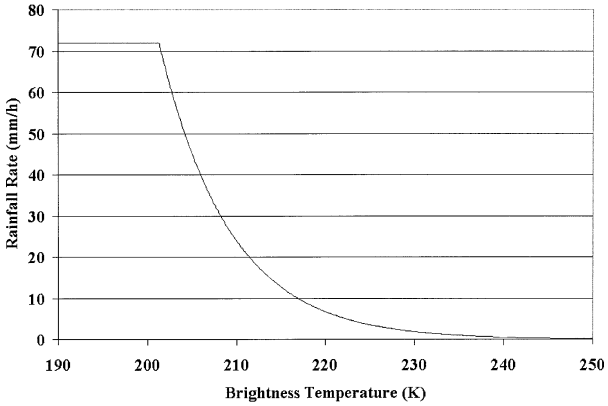

FIG. 2. Surface rainfall rate as a function of 10.7-μm brightness temperature for the Autoestimator. Note that the rain rate is capped at a maximum value of 72 mm h^{-1}.

The AE is used to produce real-time estimates of both instantaneous rainfall rates and accumulations over 1, 3, 6, and 24 h. At the time of writing, these estimates could be accessed online at the NOAA/NESDIS flash-flood home page (http://orbit35i.nesdis.noaa.gov/arad/ht/ff). The reader is referred to Vicente et al. (1998, 2002) for additional details on the AE.

The dependence of the AE on radar is a significant problem, because one of the advertised strengths of satellite QPE is its usefulness in regions for which radar and/or rain gauge coverage are unavailable. In response to this and other concerns, another version of the AE, called the Hydroestimator (Kuligowski et al. 2003, manuscript submitted to *Wea. Forecasting*), has been developed with three significant new features:

1) Raining pixels are defined as those with 10.7-μm brightness temperatures below the average value for

TABLE 1. Statistics for satellite-estimated rainfall compared with rain gauge observations for Tropical Storm Allison during the 24 h ending 1200 UTC 6 Jun 2001, for the region indicated in Fig. 4.

Algorithm	Additive bias (mm)	Adjusted rmse (mm)	Correlation coef
AE	−18.3	25.8	0.69
HE	−11.7	27.0	0.64
HE(R)	−17.9	27.6	0.62
Blended	−20.7	28.2	0.59
GMSRA1	−9.5	28.2	0.59
GMSRA2	−10.8	28.1	0.59

TABLE 2. Statistics for satellite-estimated rainfall compared with the Stage-III product for an MCS over WV during the 6 h ending 1800 UTC 8 Jul 2001.

Algorithm	Additive bias (mm)	Adjusted rmse (mm)	Correlation coef
AE	7.6	15.8	0.79
HE	1.4	12.2	0.71
HE(R)	1.1	12.2	0.72
Blended	−0.8	10.2	0.73
GMSRA1	4.0	12.8	0.53
GMSRA2	3.9	12.8	0.54

a predetermined region surrounding the pixel of interest. This approach has substantially reduced the exaggeration of rain area exhibited by the AE, which, in turn, has eliminated the need for radar as a rain/no-rain discriminator. Therefore unlike the AE, the HE can be applied outside of regions of radar coverage without compromising accuracy.

2) The standard AE rain-rate curve is adjusted according to the difference between the pixel brightness temperature and the average value in the surrounding region, with the highest rain rates assigned to pixels that are coldest relative to their surroundings.
3) The components of the PW × RH adjustment have been separated, with the PW value used to adjust the rain-rate curve based on moisture availability and the RH value used to derive an amount to be subtracted from the rain rate. These adjustments have improved the handling of stratiform events with embedded convection, and also of wintertime precipitation, which is typically associated with low PW values.

In June of 2001, the AE became operational and began to replace some of the functions of the IFFA, especially for convective events. SAB meteorologists have indicated that the AE has greatly increased their productivity: they can monitor a greater number of heavy-rainfall systems than before and can disseminate a greater number of satellite-precipitation-estimation messages (SPENES) in a more timely fashion than before. In some cases, SPENES are issued prior to the actual onset of flooding, allowing National Weather Service (NWS) Forecast Offices to issue appropriate warnings in a timely fashion. Especially useful is the looping of 1- and 3-h totals for detecting trends, movement, and propagation. Though the performance of the AE is slightly superior to that of the HE by some measures (see Tables 1 and 2), the HE was recently chosen for implementation on AWIPS. This is, in part, because the NWS Office of Hydrologic Development has a requirement for SPEs that are outside the area of radar coverage, making the AE, with its dependence on radar, inappropriate for their applications.

As a cautionary note, experience and validation studies (Kuligowski et al. 2001) have shown the following tendencies of IR-based SPEs:

1) SPEs tend to overestimate the area and magnitude of rainfall for slow-moving, large cold-topped MCSs. This overestimation can be aggravated when accumulating the estimates over many hours.
2) SPEs tend to underestimate rainfall from warm-topped MCSs (warmer than −60°C).
3) SPEs mislocate estimates in regions of strong vertical wind shear.
4) SPEs do not handle rain bursts early in the MCS life cycle [in which ≥2 in. (51 mm) of rain can occur in 0.5 h].

c. GOES multispectral rainfall algorithm

In an attempt to glean precipitation information from all five GOES channels, GMSRA was developed by Ba and Gruber (2001). Some of the properties of GMSRA were obtained from satellite-based microphysical cloud studies by Rosenfeld and Gutman (1994) and Rosenfeld and Lensky (1998). The five GOES channels are used as follows:

1) A threshold albedo value (0.4) from the visible channel is used to screen out thin cirrus, along with brightness temperature differences between 10.7 and 12.0 μm exceeding 1 K.
2) Differences between the 6.9- and 10.7-μm brightness temperature are used to distinguish overshooting tops from anvil cirrus.
3) A 3.9-μm reflectance derived from 3.9-, 10.7-, and 12.0-μm radiance data during the daylight hours is related to cloud particle size, and clouds with large particles (effective radius exceeding 15 μm) are considered to be raining even for relatively warm cloud-top brightness temperatures.
4) Changes in 10.7-μm brightness temperature are used to infer cloud growth rate and to screen out nonraining (warming) clouds.

Once the cloud screening is performed, both the probability of precipitation and the conditional rain rate are computed from the 10.7-μm brightness temperature with different calibrations for different regions. An adjustment for subcloud evaporation similar to that used in the AE (PW × RH) is also made. The reader is

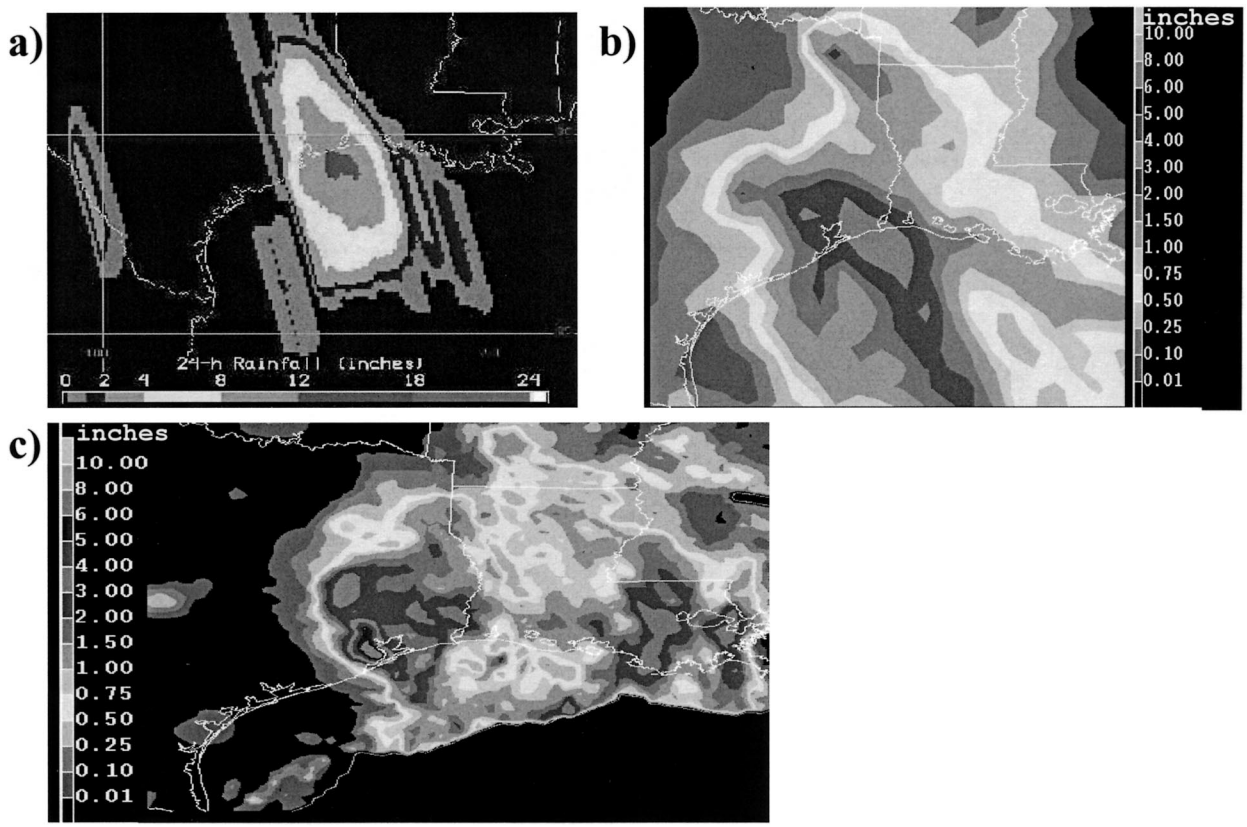

FIG. 3. Comparison of (a) TRaP (in.) (b) Eta Model QPF, and (c) Stage-III multisensor observations for the 24 h ending 1200 UTC 6 Jun 2001. The maximum rainfall amounts were ~12.5 in. (312 mm) for TRaP, >3 in. (75 mm) for the Eta Model, and ~12 in. (300 mm) for Stage III.

referred to Ba and Gruber (2001) for additional details on these adjustments and on GMSRA in general.

A nighttime cloud screening has also been introduced to GMSRA on an experimental basis. At night, clouds are considered to be raining only if the difference between 10.7 and 12.0 μm is below a certain threshold value and the difference between 3.9 and 10.7 μm exceeds a certain threshold.

4. Examples and algorithm intercomparison

This section includes a comparison of several satellite rainfall algorithms, discussed earlier, for two distinct types of extreme rainfall events: a tropical storm (Allison) and an MCS. For the former, an application of the TRaP technique is also illustrated. In addition, a broader analysis from nearly 2 yr of archived data is also presented.

a. Tropical Storm Allison (5–6 June 2001)

Tropical Storm Allison produced extremely heavy rainfall from eastern Texas across the Gulf States and along the mid-Atlantic Coast, resulting in the most extensive flooding ever associated with a tropical storm. In the Houston, Texas, metropolitan area, more than 30 in. (750 mm) of rain were reported at several locations, with at least 22 fatalities and nearly $2 billion in estimated damage associated with the storm.

Forecasting rainfall from landfalling tropical storms is extremely challenging. First of all, while a storm is offshore, the only reliable source of precipitation information comes from GOES- and microwave-based SPE. Furthermore, numerical weather prediction models normally are not able to predict the extreme rainfall accompanying tropical storm landfall. As a consequence, as described in section 2b, SAB has experimentally used the operational SSM/I rain-rate product to produce a rainfall potential for tropical disturbances expected to make landfall within 24 h (World Meteorological Organisation 1999). TRaP was recently entirely automated (Kidder et al. 2000; 2001; Ferraro et al. 2002) by using the track forecast from the Tropical Prediction Center and rain-rate data accessed from SSM/I, AMSU, and TRMM. Figure 3 shows an example in which the TRaP algorithm used rain rates from AMSU-B to calculate the onshore rainfall approximately 24 h prior to landfall. In this case, the TraP calculation predicted a 12.5-in. (312 mm) maximum along the southeast coast of Texas; approximately 12 in. (300 mm) was

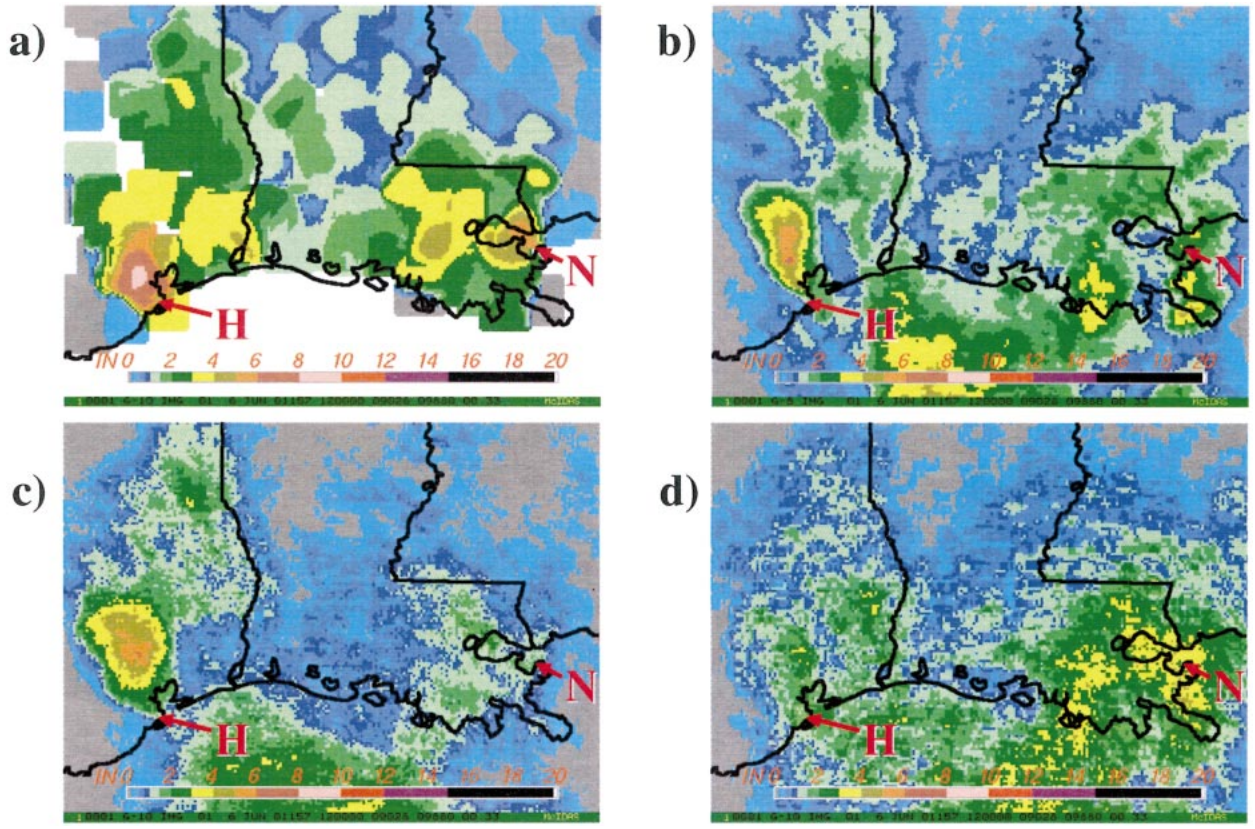

FIG. 4. Comparison of rainfall (in.) from (a) gauges, (b) the Hydroestimator, (c) the modified Turk technique, and (d) GMSRA with nighttime rain screening for the 24 h ending 1200 UTC 6 Jun 2001. The precipitation maximum near Houston, TX, is indicated by the letter N indicates a secondary maximum near New Orleans, LA.

observed. The Eta Model maximum QPF was around 3 in. (75 mm).

Table 1 is an example of ongoing validation being performed at NESDIS for a number of GOES and GOES–POES precipitation algorithms (Kuligowski et al. 2001). The NESDIS verification program has initially compared six variations of four satellite precipitation algorithms: the AE, HE, HE(R) (a version of the HE that uses a radar to screen out nonraining cloud pixels), ''blended'' (the modified Turk GOES/microwave algorithm), GMSRA1 (the original version) and GMSRA2 (the version with the additional nighttime rain/no-rain screen). Table 1 displays 24-h validation statistics, using rain gauges from the cooperative observer network as ''ground truth.'' In this example, the AE had the lowest adjusted rmse (which is the rmse with the bias component removed) and highest correlation with observed amounts, with the HE performing somewhat less well by these measures but outperforming the remaining four algorithms. The HE and the two versions of GMSRA had the least bias, however.

Estimated 24-h precipitation totals from the operational HE, GMSRA2, and the blended GOES/microwave are compared with corresponding 24-h observed rain gauge amounts in Fig. 4. Even though all three satellite algorithms underestimated the observed rainfall, the HE and blended methods depicted the patterns and cores of heavy precipitation associated with marginally cold cloud tops (around −60°C) near Houston (indicated by the letter H). GMSRA produced a relatively poor depiction of the rainfall amounts in this region; however, GMSRA performed better then the other algorithms in southeast Louisiana (around New Orleans at N), a region associated with mostly warmer tops (above −60°C) and hence more suited for GMSRA, which uses all five GOES channels to improve rainfall estimates for stratiform and warm-top convective clouds.

b. Mesoscale convective system producing devastating floods over West Virginia (8–9 July 2001)

Devastating flash floods occurred in southern West Virginia and eastern Kentucky on 8–9 July 2001. As many as 3000 homes were damaged or destroyed by flooding and mudslides; three people were killed in the most costly flood in West Virginia history.

For flash floods, algorithms must be validated over shorter time periods (less than 24 h) given the short time scales of these events. Table 2 compares the six SPE

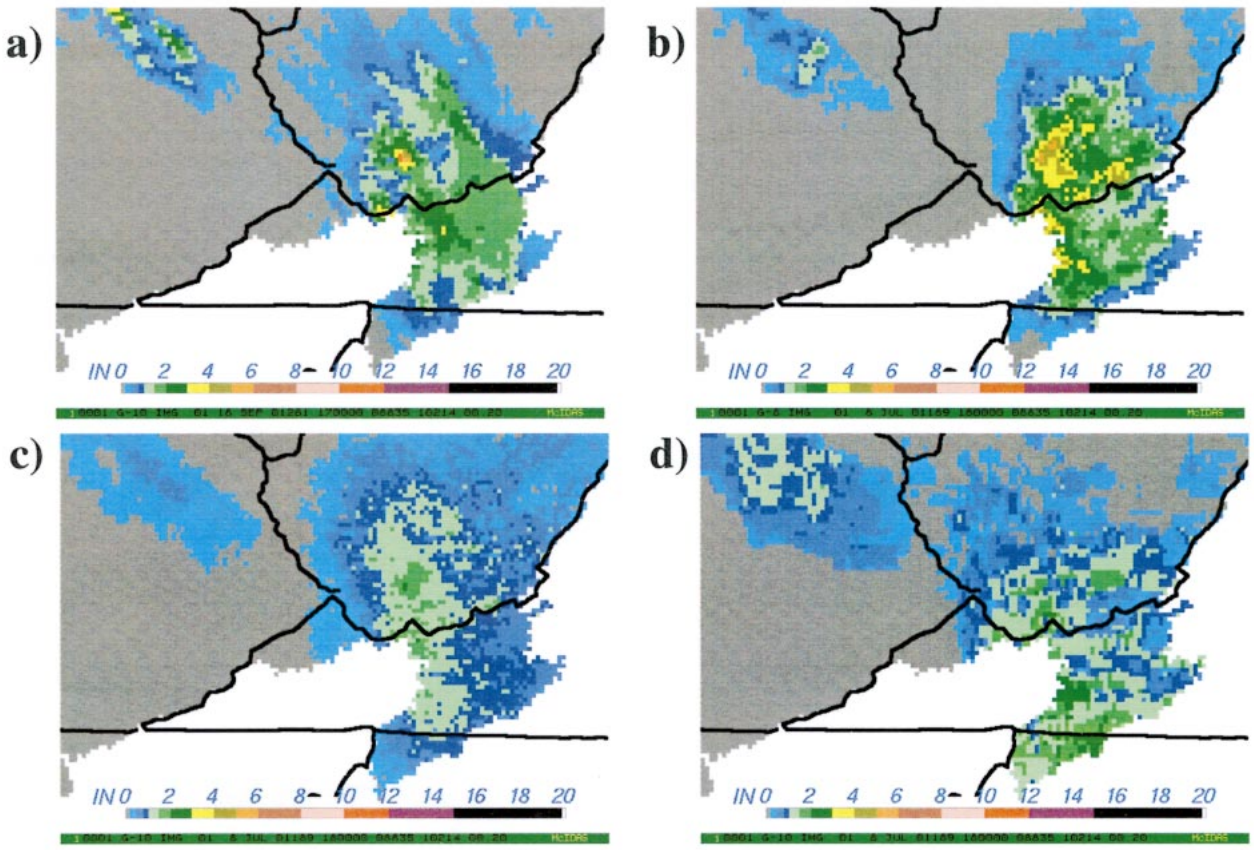

FIG. 5. Comparison of rainfall estimates (in.) from (a) Stage III, (b) the Hydroestimator, (c) the modified Turk technique, and (d) GMSRA with nighttime rain screening for the 6 h ending 1800 UTC 8 Jul 2001.

algorithms with 6-h totals from Stage-III radar–rain gauge data (Fulton et al. 1998) as ground truth. As with Allison, the AE had the highest correlation with observations, but for this event the AE also showed a strong wet bias and had the highest adjusted rmse of the group. The HE and the blended algorithms had minimal bias and correlations that were only slightly below that of the AE, resulting in significantly lower rmse values than the AE had. GMSRA estimates exhibited significantly poorer correlations with observations than did the other four estimates.

Figure 5 compares the operational HE, blended GOES/microwave, and GMSRA2 with corresponding 6-h Stage-III radar–rain gauge totals. The flash flood resulted from a slow-moving cold-top MCS event in which the cloud-top temperatures were below −70°C. In this case, the spatial pattern of the heaviest Stage-III rainfall amounts corresponded well with the HE. The HE did underestimate the peak rainfall amount by about one-half when compared with Stage III—5.12 in. (130.0 mm) versus 10.17 in. (258.5 mm)—but had a much larger region of rainfall exceeding 3 in. (76.2 mm) than did the Stage-III estimates. It is possible that the HE overestimated the areal extent of the heavy rainfall; however, is also conceivable that beam block due to the mountainous terrain over southern West Virginia could have resulted in underestimation of the rainfall by the Stage-III product in portions of this region. The blended algorithm and GMSRA exhibited spatial patterns similar to the HE and Stage-III estimates but significantly underestimated the heaviest amounts relative to the Stage-III estimates [maximum amounts of 2.05 in. (52.0 mm) and 2.40 in. (61.0 mm), respectively].

c. Two-year statistical comparison

Since April of 2001, NESDIS personnel have archived 6-hourly precipitation estimates from six of the algorithms mentioned in this paper: the Autoestimator, the Hydroestimator (with and without a radar screen), the two versions of GMSRA, and the blended algorithm. In addition, 6-hourly Stage-III radar–rain gauge estimates and daily rain gauge data have also been collected for comparison. Comparison has been performed on a seasonal basis for two regions, defined as ''western'' [defined by the California–Nevada RFC (CNRFC) and Northwest RFC (NWRFC) coverage regions, except in summer when the Colorado Basin RFC (CBRFC) re-

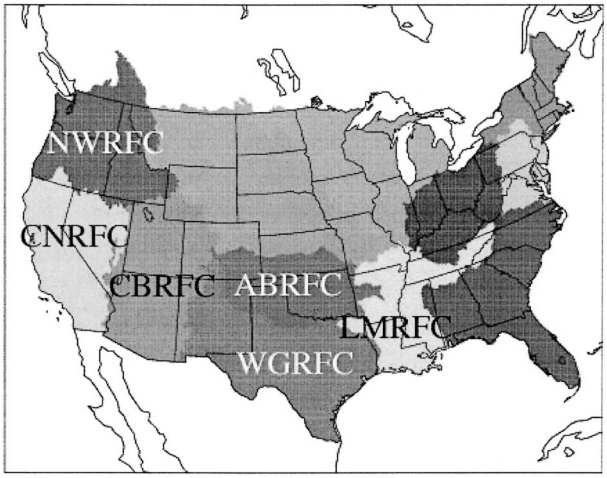

FIG. 6. RFC regions used in validation for the ''western'' (NWRFC, CNRFC, and CBRFC in place of NWRFC in summer) and ''southern plains'' (ABRFC, WGRFC, and LMRFC) regions.

places the latter to capture monsoonal precipitation], and ''central'' [defined by the Arkanasas–Red Basin RFC (ABRFC), Lower Mississippi RFC (LMRFC), and West Gulf RFC (WGRFC)]. These regions are indicated in Fig. 6. Precipitation events were subjectively divided into four types: cold-top convective (coldest tops colder than 215 K), warm-top convective (no tops colder than 215 K), stratiform, and tropical (i.e., associated with landfalling/remnant tropical systems). In addition to the comparisons of 6-h statistics, comparisons of 24-h totals with daily rain gauges are also performed to allow direct comparison with the Stage-III estimates.

For the sake of brevity, results for the nearly 2 yr (April 2001–February 2003) are presented here, without being broken down into seasons. A comparison of the bias ratio of areal coverage (the ratio of the total number of pixels with nonzero estimated rainfall to the total number of pixels with nonzero observed rainfall) is shown in Fig. 7, and the linear correlation between estimates and rain gauge observations is shown in Fig. 8. Figure 9 depicts the skill of the estimates at differentiating raining from nonraining areas with the Heidke skill score. In all three figures, the left-hand portion of

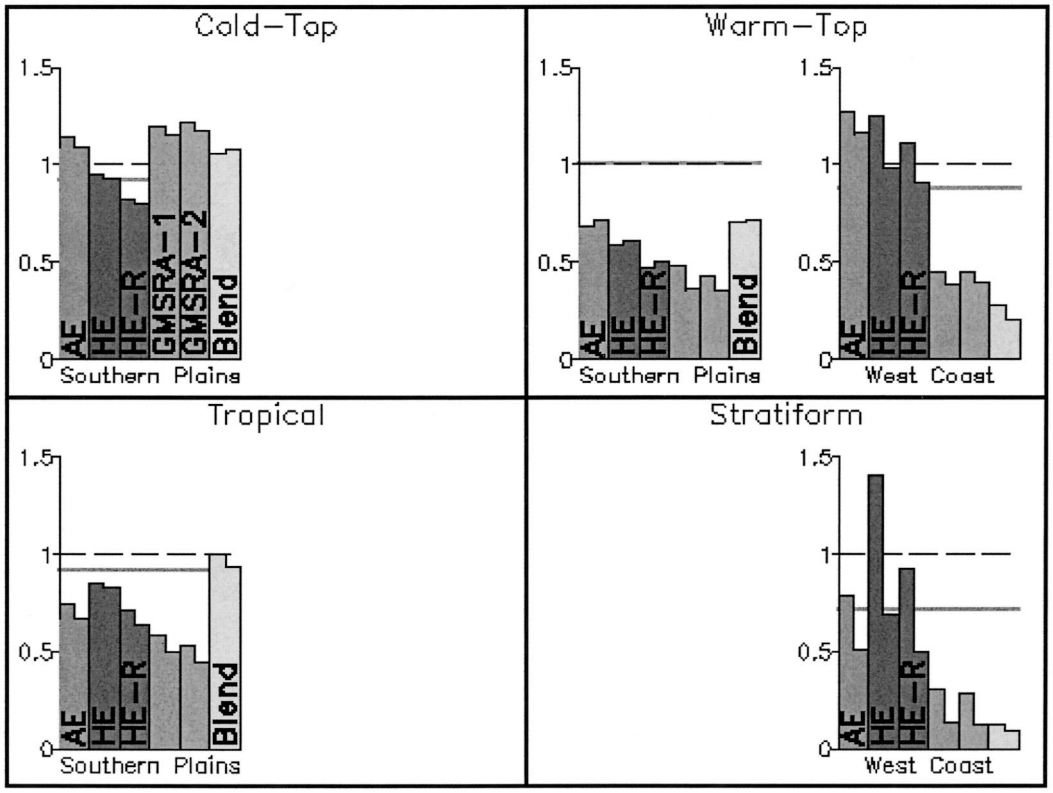

FIG. 7. Plot of bias (the ratio of the number of estimated raining pixels to the number of observed raining pixels) for the six precipitation algorithms described in this paper: Autoestimator (AE), Hydroestimator without (HE) and with a radar rain/no-rain screen (HE-R), GOES multispectral rainfall algorithm (GMSRA), and the Turk IR/microwave blended algorithm (blend). The left side of each bar represents the performance of 6-h estimates against Stage-III radar–rain gauge estimates; the right side represents the performance of 24-h estimates against rain gauges. The thick gray horizontal lines represent the corresponding values for the 24-h Stage-III estimates when compared with rain gauge values.

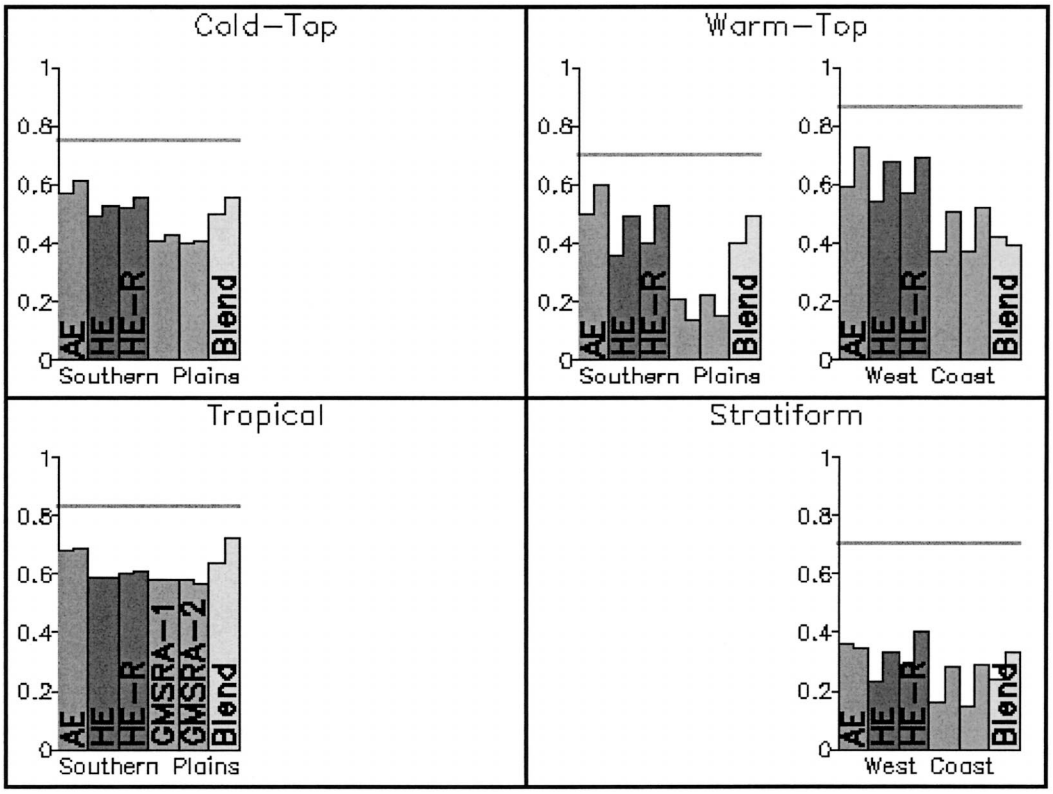

FIG. 8. Same as Fig. 7, but for linear (Pearson) correlation coefficient between estimates and observations.

each bar represents the 6-h statistical value, and the right-hand portion represents the corresponding 24-h value. A gray horizontal line indicates the corresponding 24-h value for the Stage-III data.

Although it is obvious that the Stage-III results are superior to those of the satellite algorithms, it must be kept in mind that the goal is not for satellite-based estimates to compete with radar-based estimates, but rather to complement them. Note also that the Stage-III results have been bias corrected using rain gauge data, whereas the satellite estimates have not.

All of the estimates display relatively little bias for cold-top events, which is not surprising given that they were calibrated for such events and the assumptions behind satellite QPE algorithms generally work best for cold-top events. On the other hand, dry biases of varying degrees are exhibited by the satellite QPE algorithms for warm-top, tropical, and stratiform events. [Note that the strong differences in the bias scores between the 6- and 24-h amounts for stratiform West Coast events are typical of the beam overshoot problems documented in mountainous regions (Westrick et al. 1999; Young et al. 1999)]. Overall, the AE and HE without radar are generally the least biased of the algorithms, whereas GMSRA exhibits very strong dry biases for warm-top and stratiform events.

The correlation between estimated and observed precipitation is also generally best for the AE and HE, with the blended algorithm often performing similarly and GMSRA lagging in performance. The same patterns are exhibited in the skill at discriminating raining from nonraining pixels, though the blended and GMSRA algorithms both perform poorly along the West Coast. Overall, the statistical analysis supports the decision to use the HE without radar as the operational algorithm (the AE was originally the operational algorithm but was replaced because of its dependence on radar).

5. Summary, outlook, and discussion

This paper has presented an overview of satellite QPE algorithms for both IR/visible and microwave instruments, with a focus on algorithms suited for heavy precipitation (by nature of their time and space scales) that are produced routinely at NESDIS. As demonstrated by the two case studies in section 4, satellite QPE is a useful companion to radar and rain gauges; however, much work remains to be done to improve the accuracy of SPE and produce a product that is suitable for direct incorporation into multisensor precipitation analyses, hydrologic models, and numerical models without the need for manual corrections.

A readily available avenue for improving satellite algorithms is that of calibration, especially for algorithms with fixed calibrations (e.g., the AE, HE, and GMSRA). Significant additional investment in calibration and val-

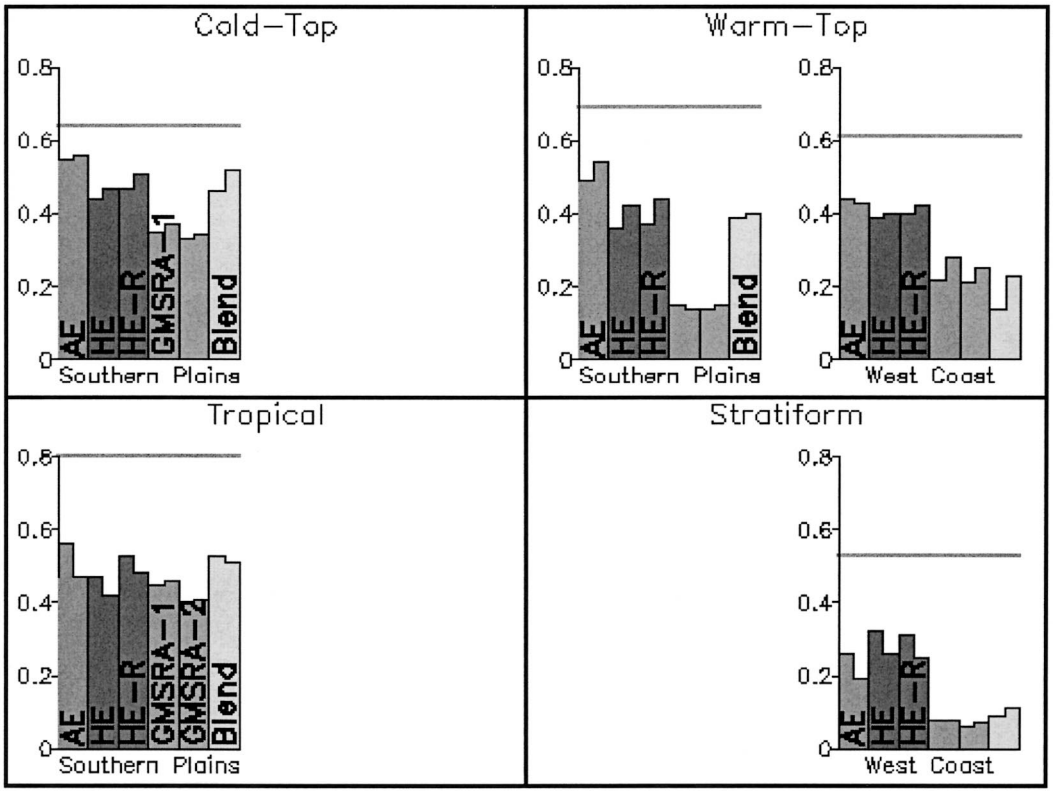

FIG. 9. Same as Fig. 7, but for Heidke skill score for rain/no-rain discrimination.

idation for different types of precipitation systems will be needed to make these algorithms more robust. This work would benefit from improvements in the availability, reliability, and timeliness of presently existing ground-truth datasets, such as the Oklahoma Mesonet. Improving the reliability of the real-time dissemination of TRMM data would also improve their usefulness in the heavy precipitation/flash-flood forecasting process.

The next generation of satellite algorithms for heavy precipitation and flash floods will make greater use of all of the GOES imager channels; GOES and POES sounding channels also need to be exploited as potential contributors for estimating precipitation. The next-generation algorithms will also use calibrated microwave precipitation estimates (which are more physically robust than IR-based estimates) to adjust GOES precipitation measurements continuously with respect to both intensity and location. Many challenges and questions remain in the development of satellite precipitation algorithms for heavy precipitation and flash floods, including

1) improving the understanding of the physical relationship between precipitation and the signals observed in the visible, IR, and microwave wavelengths and determining how best to integrate information from multiple wavelengths and instruments;
2) developing a comprehensive precipitation algorithm that uses all available information, including radar and in situ rain gauge measurements;
3) determining the best approach for algorithm development: statistical/mathematical techniques (e.g., regression, neural networks–Zhang et al. 1994; Sorooshian et al. 2000) versus physically based approaches (e.g., cloud models); and
4) discerning the best way to display the estimates: as exact values, or in terms of probability (analogous to the probabilistic QPF approach that NWS has undertaken).

In addition to improving the accuracy of SPEs, another challenge is to optimize the use of SPEs in making short-term QPF through extrapolation, because the performance of numerical weather prediction models at short lead times (0–3 h) remains inadequate (e.g., Doswell 1986). Efforts are underway at NESDIS to develop a 3-h SPE-based nowcasting algorithm that takes into account propagation characteristics of mesoscale precipitating systems (Scofield et al. 2003).

Of course, improvements in the constellation of available satellites also have the potential to improve significantly the state of satellite QPE. The launch of additional POES-based microwave instruments will increase the number of microwave passes per day, and additional channels will be introduced that could lead

to more robust retrieval algorithms. The upcoming Global Precipitation Measurement (GPM) mission promises further progress in this area by improving coordination of instrument specifications and orbit times, leading to much higher degrees of consistency and timeliness of microwave-based SPE than are available at present. In addition to GPM, a microwave radiometer is under consideration for the next generation of GOES (scheduled to begin around 2012), though the instrument would be limited to higher microwave frequencies and coarser spatial resolution than what would be offered by the GPM constellation.

The ultimate goal is to develop multisensor precipitation analyses that integrate the GOES IR-based estimates with microwave-based estimates, radar-based analyses, and in situ rain gauge measurements to produce a multispectral/multisensor algorithm for estimating precipitation from all types of precipitation systems. Quantitative precipitation estimation and segregation using multiple sensors (QPE SUMS; Gourley et al. 2002) is a good example of integrating real-time radar rainfall estimates with GOES IR-based precipitation estimates in real time. These integrated precipitation datasets can then be combined with hydrologic models and high-resolution geographic information systems data to improve the prediction of streamflow and flooding.

The future of satellite rainfall algorithms for extreme-precipitation events is exciting, because the accuracy and robustness of single-sensor and multisensor SPE algorithms continue to increase. Furthermore, global coverage of routine satellite precipitation estimates for extreme events (e.g., Alfaro and Scofield 2001) opens the way for immense potential benefits to the user community worldwide.

Acknowledgments. The authors thank Dr. Arnold Gruber and Mr. Ralph Ferraro of NESDIS, along with three anonymous reviewers for their critical review of this paper, and Mrs. Joan Reed of NESDIS for help in laying out the manuscript.

REFERENCES

Adler, R. F. and A. J. Negri, 1988: A satellite infrared technique to estimate tropical convective and stratiform rainfall. *J. Appl. Meteor.,* **27,** 30–51.

Alfaro, R., and R. A. Scofield, 2001: Validation of GOES precipitation estimates over Central America. Preprints, *11th Conf. on Satellite Meteorology and Oceanography,* Madison, WI, Amer. Meteor. Soc., 379–382.

Anagnostou, E. N., A. J. Negri, and R. F. Adler, 1999: A satellite infrared technique for diurnal rainfall variability studies. *J. Geophys. Res.,* **104,** 31 477–31 488.

Arkin, P. A., and B. N. Meisner, 1987: The relationship between large-scale convective rainfall and cold cloud over the Western Hemisphere during 1982–84. *Mon. Wea. Rev.,* **115,** 51–74.

Ba, M. B., and A. Gruber, 2001: GOES multispectral rainfall algorithm (GMSRA). *J. Appl. Meteor.,* **40,** 1500–1514.

Barrett, E. C., 1970: The estimation of monthly rainfall from satellite data. *Mon. Wea. Rev.,* **98,** 322–327.

——, and D. W. Martin, 1981: *The Use of Satellite Data in Rainfall Monitoring.* Academic Press, 340 pp.

——, C. C. Kidd, and J. O. Bailey, 1988: The Special Sensor Microwave/Imager: A new instrument with rainfall monitoring potential. *Int. J. Remote Sens.,* **9,** 1943–1950.

Borneman, R., 1988: Satellite rainfall estimating program of the NOAA/NESDIS Satellite Analysis Branch. *Natl. Wea. Dig.,* **13** (2), 7–15.

Conner, M. D., and G. W. Petty, 1998: Validation and intercomparison of SSM/I rain-rate retrieval methods over the continental United States. *J. Appl. Meteor.,* **37,** 679–700.

Corfidi, S. F., J. H. Merritt, and J. M. Fritsch, 1996: Predicting the movement of mesoscale convective complexes. *Wea. Forecasting,* **11,** 41–46.

Doswell, C. A., III, 1986: Short-range forecasting. *Mesoscale Meteorology and Forecasting,* P. S. Ray, Ed., Amer. Meteor. Soc., 689–719.

Ferraro, R. R., 1997: Special Sensor Microwave Imager derived global rainfall estimates for climatological applications. *J. Geophys. Res.,* **102,** 16 715–16 736.

——, S. J. Kusselson, and M. C. Colton, 1998: An introduction to passive microwave remote sensing and its applications. *Natl. Wea. Dig.,* **22** (3), 11–23.

——, G. Vicente, M. Ba, A. Gruber, R. Scofield, Q. Li, and R. Weldon, 1999: Satellite techniques yield insight into devastating rainfall from Hurricane Mitch. *Eos, Trans. Amer. Geophys. Union,* **80,** 505, 512, 514.

——, F. Weng, N. Grody, and L. Zhao, 2000: Precipitation characteristics over land from the *NOAA-15* AMSU sensor. *Geophys. Res. Lett.,* **27,** 2669–2672.

——, P. Pellegrino, S. Kusselson, M. Turk, and S. Kidder, 2002: Validation of SSM/I and AMSU-derived tropical rainfall potential (TraP) during the 2001 Atlantic hurricane season. NOAA Tech. Rep. NESDIS 105, 43 pp. [Available from NOAA/NESDIS Office of Research and Applications, 5200 Auth Rd., Camp Springs, MD, 20746–4304.]

Follansbee, W. A., 1973: Estimation of average daily rainfall from satellite cloud photographs. NOAA Tech. Memo. NESS 44, 39 pp. [Available from NOAA/NESDIS Office of Research and Applications, 5200 Auth Rd., Camp Springs, MD, 20746–4304.]

——, and V. J. Oliver, 1975: A comparison of infrared imagery and video pictures in the estimation of daily rainfall from satellite data. NOAA Tech. Memo. NESS 62, 14 pp.

Fulton, R. A., J. P. Breidenbach, D. J. Seo, and D. A. Miller, 1998: The WSR-88D rainfall algorithm. *Wea. Forecasting,* **13,** 377–395.

Gourley, J. J., R. A. Maddox, K. W. Howard, and D. W. Burgess, 2002: An exploratory multisensor technique for quantitative estimation of rainfall. *J. Hydrometeor.,* **3,** 166–180.

Griffith, C. G., W. L. Woodley, P. G. Grube, D. W. Martin. J. Stout, and D. N. Sikdar, 1978: Rain estimates from geosynchronous satellite imagery: Visible and infrared studies. *Mon. Wea. Rev.,* **106,** 1153–1171.

Groisman, P. Ya., and D. R. Legates, 1994: The accuracy of United States precipitation data. *Bull. Amer. Meteor. Soc.,* **75,** 215–227.

Huffman, G. J., R. F. Adler, M. M. Morrissey, D. T. Bolvin, S. Curtis, R. Joyce, B. McGavock, and J. Susskind, 2001: Global precipitation at one-degree daily resolution from multisatellite observations. *J. Hydrometeor.,* **2,** 36–50.

Hunter, S. M., 1996: WSR-88D radar rainfall estimation: Capabilities, limitations, and potential improvements. *Natl. Wea. Dig.,* **20** (4), 26–38.

Juying, X., and R. A. Scofield, 1989: Satellite-derived rainfall estimates and propagation characteristics associated with mesoscale convective systems (MCS). NOAA Tech. Memo. NESDIS 25, 49 pp.

Kidder, S. Q., M. D. Goldberg, R. M. Zehr, R. M. DeMaria, J. F. W. Purdom, C. S. Velden, N. C. Grody, and S. J. Kusselson, 2000: Satellite analysis of tropical cyclones using the Advanced Microwave Sounding Unit (AMSU). *Bull. Amer. Meteor. Soc.,* **81,** 1241–1259.

——, S. J. Kusselson, J. A. Knaff, and R. J. Kuligowski, 2001: Improvements to the experimental tropical rainfall potential (TRaP) technique. Preprints, *11th Conf. on Satellite Meteorology and Oceanography*, Madison, WI, Amer. Meteor. Soc., 375–378.

Kitchen, M., and P. M. Jackson, 1993: Weather radar performance at long range—Simulated and observed. *J. Appl. Meteor.*, **32,** 975–985.

Kuligowski, R. J., 1997: An overview of National Weather Service quantitative precipitation estimates (QPE). Techniques Development Laboratory Office Note 97-4, 27 pp. [Available from NOAA/NWS Meteorological Development Laboratory, 1325 East–West Hwy., Silver Spring, MD 20910–3283.]

——, 2002: A self-calibrating GOES rainfall algorithm for short-term rainfall estimates. *J. Hydrometeor.*, **3,** 112–130.

——, S. Qiu, R. A. Scofield, and A. Gruber, 2001: The NESDIS QPE verification program. Preprints, *11th Conf. on Satellite Meteorology and Oceanography*, Madison, WI, Amer. Meteor. Soc., 383–384.

Kummerow, C., W. Barnes, T. Kozu, J. Shiue, and J. Simpson, 1998: The Tropical Rainfall Measuring Mission (TRMM) sensor package. *J. Atmos. Oceanic Technol.*, **15,** 809–817.

——, and Coauthors, 2001: The evolution of the Goddard profiling algorithm (GPROF) for rainfall estimation from passive microwave sensors. *J. Appl. Meteor.*, **40,** 1801–1820.

Lethbridge, M., 1967: Precipitation probability and satellite radiation data. *Mon. Wea. Rev.*, **95,** 487–490.

Manobianco, J., S. Koch, V. M. Karyampudi, and A. J. Negri, 1994: The impact of assimilating satellite-derived precipitation rates on numerical simulations of the ERICA IOP 4 cyclone. *Mon. Wea. Rev.*, **122,** 341–365.

Miller, S. W., P. A. Arkin, and R. Joyce, 2001: A combined microwave/infrared rain rate algorithm. *Int. J. Remote Sens.*, **22,** 3285–3307.

Peck, E. L., 1997: Quality of hydrometeorological data in cold regions. *J. Amer. Water Resour. Assoc.*, **33,** 125–134.

Petty, G. W., 1995: The status of satellite-based rainfall estimation over land. *Remote Sens. Environ.*, **51,** 125–137.

——, and W. Krajewski, 1996: Satellite rainfall estimation over land. *Hydrol. Sci. J.*, **41,** 433–451.

Rosenfield, D., and G. Gutman, 1994: Retrieving microphysical properties near the tops of potential rain clouds by multi spectral analysis of AVHRR data. *Atmos. Res.*, **34,** 259–283.

——, and I. Lensky, 1998: Satellite-based insights into precipitation formation processes in continental and maritime convective clouds. *Bull. Amer. Meteor. Soc.*, **79,** 2457–2476.

Savage, R. C., and J. A. Weinman, 1975: Preliminary calculations of the upwelling radiance from rainclouds at 37.0 and 19.35 GHz. *Bull. Amer. Meteor. Soc.*, **56,** 1272–1274.

Scofield, R. A., 1987: The NESDIS operational convective precipitation estimation technique. *Mon. Wea. Rev.*, **115,** 1773–1792.

——, 1991: Operational estimation of precipitation from satellite data. *Palaeogr. Palaeoclimatol. Palaeoecol.*, **90,** 79–86.

——, 2001: Comments on ''A quantitative assessment of the NESDIS Auto-Estimator.'' *Wea. Forecasting*, **16,** 277–278.

——, and V. J. Oliver, 1977: A scheme for estimating convective rainfall from satellite imagery. NOAA Tech. Memo. NESS 86, 47 pp.

——, and L. E. Spayd Jr., 1984: A technique that uses satellite, radar, and conventional data for analyzing and short-range forecasting of precipitation from extratropical cyclones. NOAA Tech. Memo. NESDIS 8, 51 pp.

——, M. DeMaria, and R. Alfaro, 2001: Space-based rainfall capabilities in hurricanes offshore and inland. Preprints, *Symp. on Precipitation Extremes: Prediction, Impacts, and Response*, Albuquerque, NM, Amer. Meteor. Soc., 297–301.

——, R. J. Kuligowski, and C. Davenport, 2003: From satellite quantitative precipitation estimates (QPE) to nowcasts for extreme precipitation events. Preprints, *17th Conf. on Hydrology*, Long Beach, CA, Amer. Meteor. Soc., CD-ROM, J4.2.

Seo, D. J., and J. P. Breidenbach, 2002: Real-time correction of spatially nonuniform bias in radar rainfall data using rain gauge measurements. *J. Hydrometeor.*, **3,** 93–111.

——, ——, R. Fulton, and D. Miller, 2000: Real-time adjustment of range-dependent biases in WSR-88D rainfall estimates due to nonuniform vertical profile of reflectivity. *J. Hydrometeor.*, **1,** 222–240.

Shi, J., and R. A. Scofield, 1987: Satellite observed mesoscale convective system (MCS) propagation characteristics and a 3–12 hour heavy precipitation forecast index. NOAA Tech. Memo. NESDIS 20, 43 pp.

Smith, E. A., and Coauthors, 1998: Results of WetNet PIP-2 project. *J. Atmos. Sci.*, **55,** 1483–1536.

Smith, J. A., A. A. Bradley, and M. L. Baeck, 1994: The space–time structure of extreme storm rainfall in the southern plains. *J. Appl. Meteor.*, **33,** 1402–1417.

——, D.-J. Seo, M. L. Baeck, and M. D. Hudlow, 1996: An intercomparison study of NEXRAD precipitation estimates. *Water Resour. Res.*, **32,** 2035–2045.

Sorooshian, S., K.-L. Hsu, X. Gao, H. V. Gupta, B. Imam, and D. Braithwaite, 2000: An evaluation of PERSIANN system satellite-based estimates of tropical rainfall. *Bull. Amer. Meteor. Soc.*, **81,** 2035–2046.

Spayd, L. E., Jr., and R. A. Scofield, 1984a: A tropical cyclone precipitation estimation technique using geostationary satellite data. NOAA Tech. Memo. NESDIS 5, 36 pp.

——, and ——, 1984b: An experimental satellite-derived heavy convective rainfall short range forecasting technique. Preprints, *10th Conf. on Weather Forecasting and Analysis*, Clearwater Beach, FL, Amer. Meteor. Soc., 400–408.

Spencer, R. W., 1986: A satellite pasive 37-GHz scattering-based method for measuring oceanic rain rates. *J. Climate Appl. Meteor.*, **25,** 754–766.

——, H. M. Goodman, and R. E. Hood, 1989: Precipitation retrieval over land and ocean with the SSM/I: Identification and characteristics of the scattering signal. *J. Atmos. Oceanic Technol.*, **6,** 254–273.

Todd, M. C., C. Kidd, D. Kniveton, and T. J. Bellerby, 2001: A combined satellite infrared and passive microwave technique for estimation of small-scale rainfall. *J. Atmos. Oceanic Technol.*, **18,** 742–755.

Turk, F. J., F. S. Marzano, and E. A. Smith, 1998: Combining geostationary and SSM/I data for rapid rain rate estimation and accumulation. Preprints, *Ninth Conf. on Satellite Meteorology and Oceanography*, Paris, France, Amer. Meteor. Soc., 462–465.

Vicente, G., 1994: Hourly retrieval of precipitation rate from the combination of passive microwave and IR satellite radiometric measurements. Ph.D. dissertation, University of Wisconsin, 127 pp.

——, R. A. Scofield, and W. P. Menzel, 1998: The operational GOES infrared rainfall estimation technique. *Bull. Amer. Meteor. Soc.*, **79,** 1883–1898.

——, J. C. Davenport, and R. A. Scofield, 2002: The role of orographic and parallax corrections on real time high resolution satellite rainfall rate distribution. *Int. J. Remote Sens.*, **23,** 221–230.

Weinman, J. A., and P. J. Guetter, 1977: Determination of rainfall distributions from microwave radiation measured by the *Nimbus 6* EMSR. *J. Appl. Meteor.*, **16,** 437–442.

Weng, F., L. Zhao, R. R. Ferraro, G. Poe, X. Li, and N. C. Grody, 2003: Advanced Microwave Sounding Unit (AMSU) cloud and precipitation algorithms. *Radio Sci.*, **38,** 8086–8096.

Westrick, K. J., C. F. Mass, and B. A. Colle, 1999: The limitations of the WSR-88D radar network for quantitative precipitation measurement over the western United States. *Bull. Amer. Meteor. Soc.*, **80,** 2289–2298.

World Meteorological Organization, 1999: Estimating the amount of rainfall associated with tropical cyclones using satellite techniques. WMO/TD No. 975, TCP-42, 294 pp.

Young, C. B., B. R. Nelson, A. A. Bradley, J. A. Smith, C. D. Peters-Lidard, A. Kruger, and M. L. Baeck, 1999: An evaluation of NEXRAD precipitation estimates in complex terrain. *J. Geophys. Res.*, **104,** 19 691–19 703.

——, A. A. Bradley, W. F. Krajewski, A. Kruger, and M. L. Morrissey, 2000: Evaluating NEXRAD multisensor precipitation estimates for operational hydrologic forecasting. *J. Hydrometeor.*, **1,** 241–254.

Zhang, M., and R. A. Scofield, 1994: Artificial neural network techniques for estimating convective rainfall and recognizing cloud mergers from satellite data. *Int. J. Remote Sens.*, **15,** 3241–3261.